Circulation and water masses beneath the northern Ronne Ice Shelf, Antarctica

Keith W. Nicholls and Keith Makinson
British Antarctic Survey, Natural Environmental Research Council, Cambridge, UK

Svein Østerhus
Bjerknes Centre for Climate Research, University of Bergen, Bergen, Norway

Received 29 January 2004; revised 6 September 2004; accepted 19 October 2004; published 14 December 2004.

[1] We present oceanographic data from beneath the northern Ronne Ice Shelf. The data were collected during the austral summer of 2002–2003 from four sites located near the ice front in the Ronne Depression. They consist of conductivity-temperature-depth (CTD) profiles and time series from moored instruments that vary in length from 9 to 20 weeks. A strong, tidally modulated inflow of relatively fresh water was found at the eastern margin of the Ronne Depression. This low-density inflow powers high basal melt rates that are responsible for a substantially thinned area of ice shelf. A northward flow of Ice Shelf Water along the western margin of the depression (the Antarctic Peninsula coast) was inferred from the CTD data. From the new CTD and current meter data, and from published results from cruises along the ice front, we suggest that the flows at the margins of the Ronne Depression establish east-west density gradients that drive an anticyclonic circulation within the depression. The barotropic component of the circulation forms a gyre of strength 5×10^5 m^3 s^{-1} and occupies a bowl in the field of water column thickness in the northern portion of the depression. All water masses sampled had temperatures below the surface freezing point and are therefore classified as Ice Shelf Water. The relatively complex nature of the oceanographic regime in the Ronne Depression is overlain by a seasonal variability that is hinted at by the available time series, probably explaining the apparent absence of inflowing HSSW at the time of the measurements. *INDEX TERMS:* 4207 Oceanography: General: Arctic and Antarctic oceanography; 9310 Information Related to Geographic Region: Antarctica; 4283 Oceanography: General: Water masses; *KEYWORDS:* Antarctic ice shelves, high-salinity shelf water, circulation

Citation: Nicholls, K. W., K. Makinson, and S. Østerhus (2004), Circulation and water masses beneath the northern Ronne Ice Shelf, Antarctica, *J. Geophys. Res.*, *109*, C12017, doi:10.1029/2004JC002302.

1. Introduction

[2] Ronne Ice Shelf (RIS) is one of the largest floating ice shelves fringing the Antarctic Ice Sheet (Figure 1). Together with Filchner Ice Shelf, which lies to the east, the RIS converts in excess of 1 Sv (1 Sverdrup $\equiv 10^6$ m^3 s^{-1}) of High Salinity Shelf Water (HSSW) into Ice Shelf Water (ISW) [*Nicholls et al.*, 2003]. ISW, characterized by a temperature that is lower than the surface freezing point (~ -1.9°C), is able to descend the continental slope to contribute to the production of Weddell Sea deep and bottom waters, precursors to Antarctic Bottom Water.

[3] A two-dimensional schematic of the processes involved in the conversion of HSSW to ISW is shown in Figure 2. In polar waters the density of the seawater is primarily governed by salinity. HSSW, which is formed by brine rejection during sea-ice production, is therefore a relatively dense water mass that is able to descend beneath the ice shelf, finally encountering the ice shelf base at depths in excess of 1500 m. Even though the water is initially at the surface freezing point, the depression of the freezing point with pressure means that at 1000 dbar, for example, HSSW is 0.74°C warmer than the freezing point of ice [*Millero*, 1978]. Rapid melting can therefore take place when deep basal ice is exposed to HSSW. The ISW that results from the addition of cold meltwater to HSSW is relatively buoyant, and it ascends the ice shelf base. Melting continues for as long as the ascending ISW entrains sufficient warm water from beneath to maintain it at a temperature higher than the freezing point. If, however, the increasing freezing temperature overtakes the plume temperature, the ISW becomes in situ supercooled, and frazil ice is likely to form. Under these circumstances, and when the turbulence in the water is low enough, the ice crystals ascend to the ice shelf base and accrete to form a layer of marine ice. On RIS the marine ice layer can constitute up to half the total ice shelf thickness [*Thyssen et al.*, 1993]. The combination of entrainment of HSSW and deposition of marine ice causes an increase in ISW density. This, together

0148-0227/04/2004JC002302$09.00

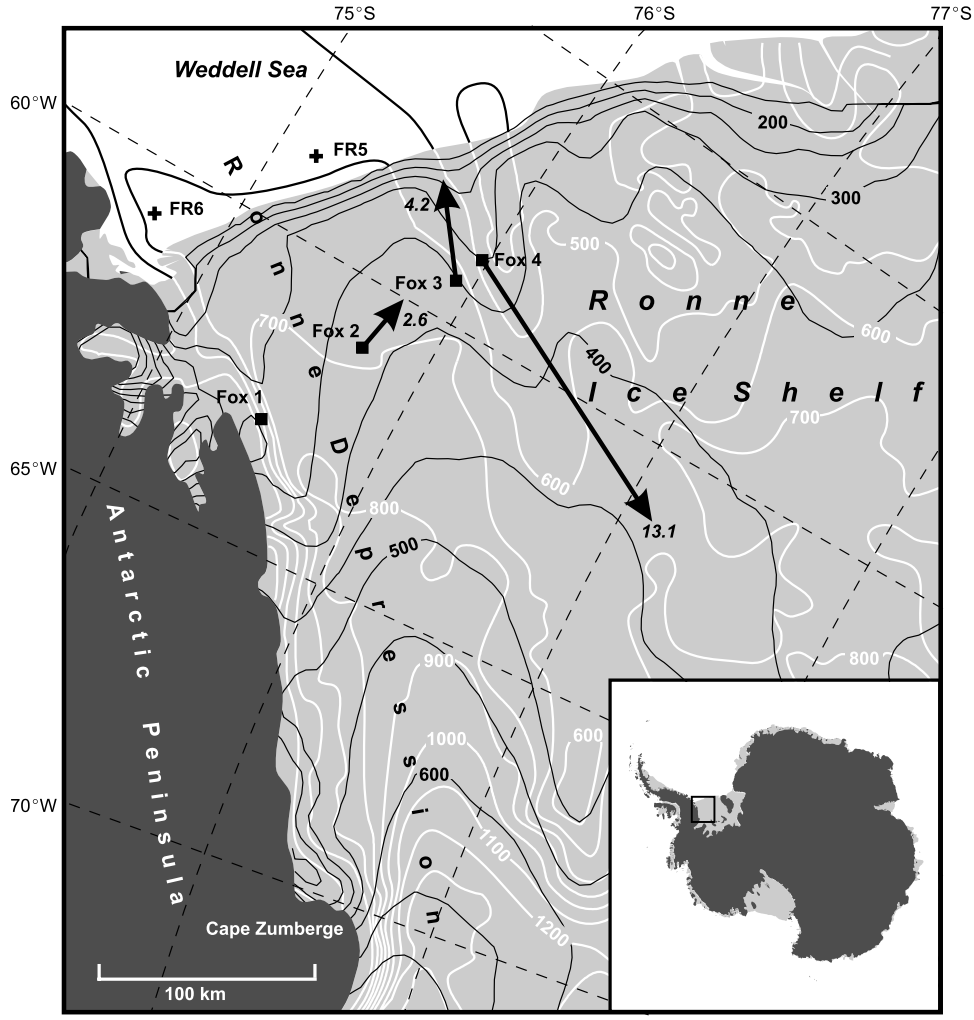

Figure 1. Map showing the northern Ronne Ice Shelf. The white contours indicate the bedrock depth below sea level in meters, with a 100-m contour interval [*Vaughan et al.*, 1994]. The black contours are ice shelf thickness in meters, with a 50-m contour interval [*Lythe and Vaughan*, 2001]. FR5 and FR6 are the sites of ice front instrument moorings mentioned in the text. The locations of the Fox sites are indicated, as are the time and depth-averaged currents measured at Fox 2, 3, and 4. The velocity magnitudes are indicated in cm s^{-1} beside each arrowhead. The 2-month period over which the currents are averaged is the same for each site. No current data are available for Fox 1.

with effects of local topography, can result in some of the ISW recirculating toward the grounding line, creating an internal circulation cell driven by the difference in freezing point between the deep and shallow parts of the ice shelf base [*Gerdes et al.*, 1999; *Nicholls et al.*, 2001].

[4] Regardless of the processes beneath the ice shelf, the outflow of ISW at the ice front must have the same flux as the HSSW inflow, enhanced slightly by the admixture of glacial melt. ISW north of Filchner Ice Shelf has been observed flowing down the continental slope with a flux of the order of 1 Sverdrup [*Foldvik et al.*, 1985], but what controls the strength of the flow? *Nicholls et al.* [2003] have shown that the rate of production of HSSW over the continental shelf appears not to be the primary limiting factor on the flow of HSSW into the cavity. Even at the end of summer, HSSW dominates the Ronne Depression north of the ice front, one of the principal regions of HSSW inflow into the sub-ice shelf cavity. A study designed to

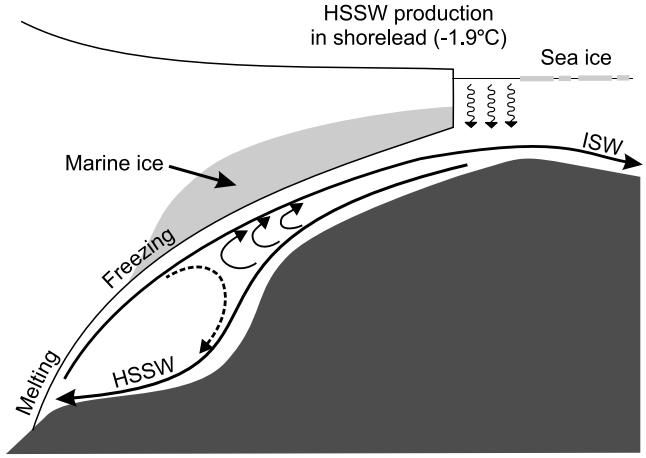

Figure 2. Two-dimensional schematic showing key sub-ice shelf oceanographic processes.

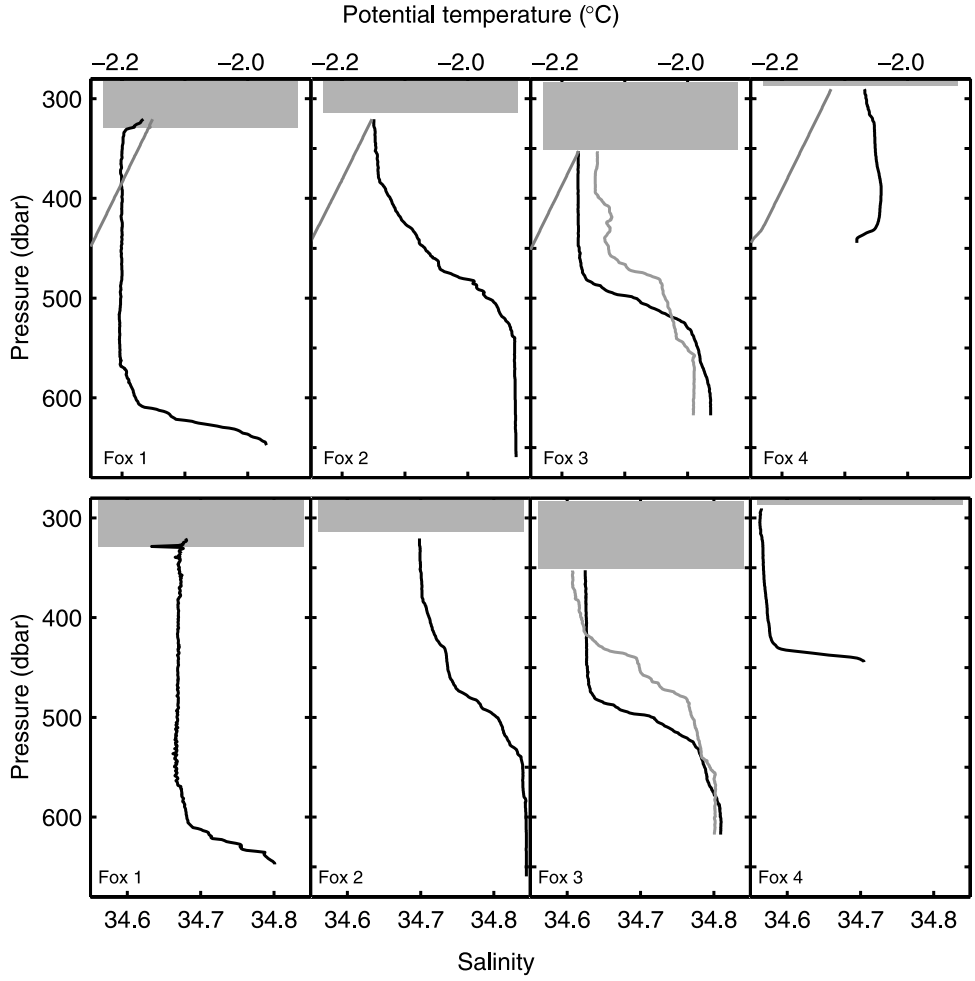

Figure 3. Profiles of (top) θ and θ_f and (bottom) *S* for each site, after averaging and depth-binning at 1-m depth intervals. The two profiles shown for Fox 3 are from the two separate visits to that site, the shaded line representing the second visit. The shaded patches represent the ice shelf.

determine the nature of the controls on the HSSW inflow will use a set of oceanographic moorings deployed across the Ronne Depression to monitor the flux of HSSW into the western end of the cavity. Between late November 2002 and mid-February 2003 a hot-water drill was used to make access holes through the ice shelf at four sites (Figure 1), allowing oceanographic instruments to be deployed. The site locations were selected to be far enough south to avoid complex dynamical effects from the presence of the large step-change in water column thickness imposed by the ice front. Using the ice shelf as a platform also offers the logistical advantage of removing the need for repeat ship visits to service moorings in a region awkward to access because of difficult sea-ice conditions. An additional advantage is that the moorings are safe from being dredged by icebergs. The principal disadvantage, of course, is the intense logistical effort involved in establishing the sites: A ship is able to obtain CTD profiles and deploy moorings at four sites in as many days, whereas the ice-shelf based project took nearly 3 months, even after all the drilling equipment and fuel had been moved into position.

[5] In this paper we present temperature and salinity profiles obtained from the drill sites, and interpret them in terms of the ice-ocean interactions at each site, the evolution of the water masses that were observed, and the more general circulation beneath the northern Ronne Ice Shelf during the middle to late austral summer. The initial few weeks of data available from three of the four moorings are presented as additional evidence for the regional circulation.

2. Measurements

[6] A short series of conductivity-temperature-depth (CTD) profiles was obtained at each of the four drill sites (Fox 1, 2, 3, and 4, Figure 1) using Idronaut Ocean Seven 319 and 320 CTD probes. Each probe carries dual temperature and conductivity sensors. A single point check on the conductivity cells was made before each set of casts using a field calibration bath. The estimated accuracy of the probes was ±0.002°C, and ±0.004 in salinity.

[7] Profiles of potential temperature (θ, top panel), salinity (*S*, bottom panel), and freezing point (θ_f, top panel) for each of the sites are shown in Figure 3. The freezing point profiles are in situ freezing points, but adjusted to potential temperatures so that they are directly comparable with the θ profiles. The data have been binned at 1-dbar intervals.

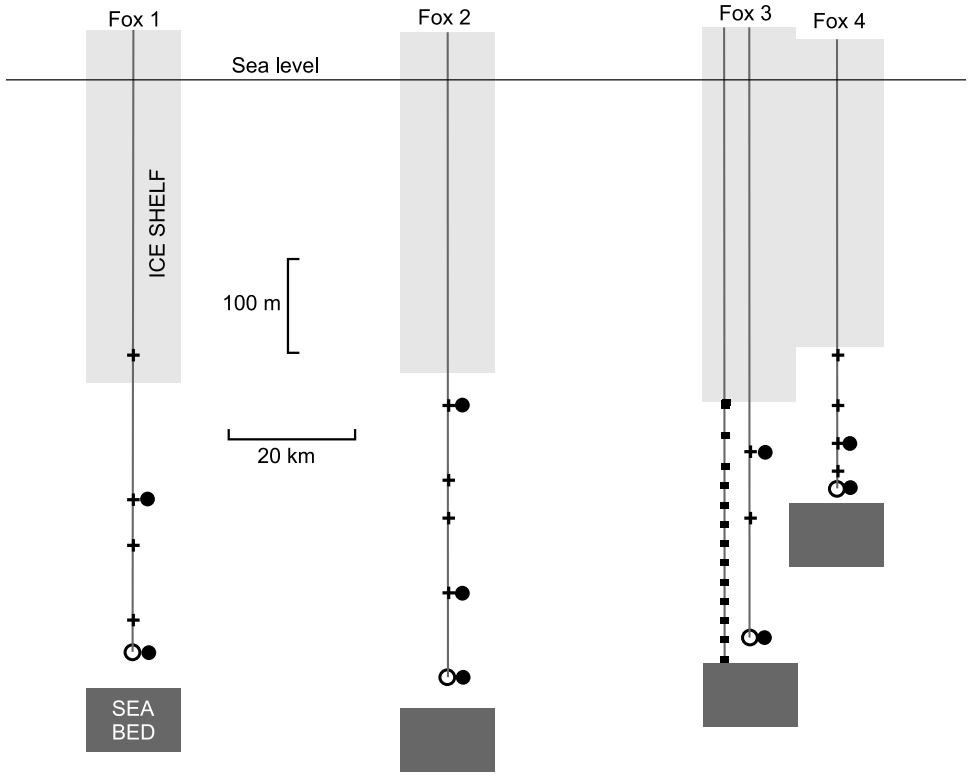

Figure 4. Diagram showing the mooring configuration at each site. Current meters (with Aanderaa RCM 9 heads): solid circles; Microcat conductivity and temperature sensors: open circles; Aanderaa-type conductivity and temperature sensors: crosses; and Pt100 element temperature sensors: squares. At Fox 1 the upper TC sensor is within the slush-filled basal crevasse.

[8] Strings of instruments were deployed at each site to provide long-term records of the oceanographic conditions. Figure 4 shows the configuration of instruments on each string. All the data are recorded on data loggers locally, with the majority also being returned via a satellite datalink. Although the transmitted data are available at this time, technical problems have limited the time series to a few months at most, with no data at all from Fox 1. The diagram in Figure 5 shows how the measurement intervals relate to each other for the three sites, and the time at which the CTD profiles were measured. Note that Fox 3 received two visits, one at the start of the field season, and again near the end; the average profiles for the two visits are shown separately in Figure 3.

[9] The time series from the mid-water instrument at Fox 2 is shown in Figure 6, which indicates that the currents in this part of the Ronne Depression are dominated by a strong semidiurnal tide. Arrows in Figure 1 show the mean current speed and direction for each instrument string, the averages being calculated using the period for which the time series from each site overlapped, namely the 2-month period for

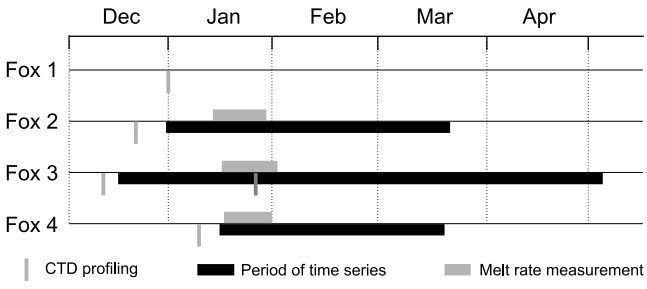

Figure 5. Diagram showing times during the season when CTD measurements were obtained, and the intervals for which data are available from moored instruments. The interval over which each melt-rate measurement was made is shown, though they were made during the previous year (2001–2002).

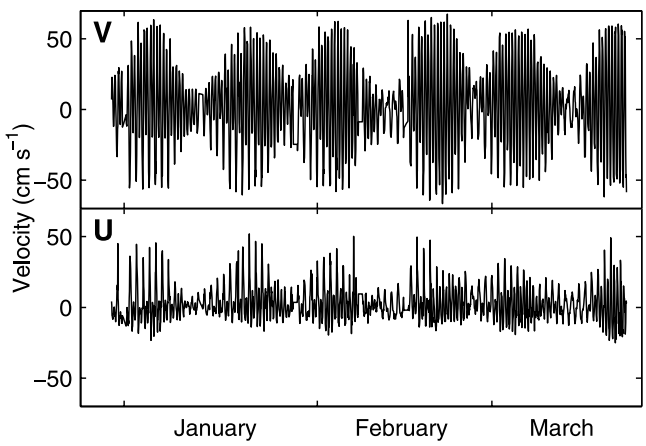

Figure 6. Time series of currents from mid-depth current meter at Fox 2. The *u* and *v* components are resolved across (140°) and along (50°) the Ronne Depression, respectively.

Table 1. Mean Currents Across (U) and Along (V) the Ronne Depression, and Mean Speed, as Measured by Current Meters at Fox 2, Fox 3, and Fox 4

Site	Pressure, dbar	Record, days	U, cm s^{-1}	V, cm s^{-1}	$\langle \lvert \underline{u} \rvert \rangle$, cm s^{-1}
Fox 2	350	82	−0.89	0.82	16.2
	550	82	2.53	1.92	25.1
	640	82	2.59	1.57	20.0
Fox 3	400	141	−0.44	3.04	18.2
	600	141	0.75	6.22	22.2
Fox 4	390	63	5.97	−11.92	35.1
	440	63	5.06	−11.77	35.1

which we have data from Fox 4. Mean velocities from the full time series available from each instrument are given in Table 1. The tidal domination of the current regime is indicated by the relatively high mean speeds that were measured at each instrument, and which are also reported in Table 1.

3. Ice-Ocean Interactions

[10] Using a combination of a phase-sensitive radar system and an ice-strain survey, direct measurements of the basal melt rate at Fox 2, 3, and 4 were obtained during the austral summer of the previous year (2001–2002). The measurement technique averaged the melt rates over a period of between 14 and 17 days, and the measurements were made at times in the season indicated in Figure 5. *Corr et al.* [2002] describe the technique in detail. The rate of melting at the base of an ice shelf depends primarily on the water speed and the amount of heat in the water column near the ice shelf base available for melting ice, that is, the amount of superheat in the water column, or the "thermal driving." Inspection of the temperature profiles in Figure 3 shows quite different thermal driving for the four sites, implying strongly differing melt rates. At the time of profiling, the water column at Fox 4 exhibited a superheating of 0.053°C, implying a relatively high basal melt rate. At this site in 2001–2002, GPS and radar gave a direct measurement of melt rate of 1.41 ± 0.08 m yr^{-1}. The water column at Fox 3, 15 km to the west, had a superheat of essentially zero during the first period of CTD profiling, implying zero basal melting at that time. However, at the time of the second visit to Fox 3 (see Figure 5), the temperature of the upper boundary layer had warmed to give a superheat of 0.031°C. As can be seen from Figure 5, this later profile was obtained relatively soon after the visit to Fox 4. For Fox 3, the direct measurement obtained in 2001–2002 gave a value of 0.0 ± 0.04 m yr^{-1}. The water column at Fox 2 showed a very modest thermal driving of 0.002°C, which, bearing in mind the accuracy of the CTD instrument, is not significantly different from zero. Again, the results from the radar measurements from the previous year yielded a correspondingly small melt rate of 0.12 ± 0.04 m yr^{-1}.

[11] During the drilling process at Fox 1, hydraulic connection was made with the sea when the nozzle depth was estimated to be around 310 m. The remainder of the ice thickness was made up of slushy ice, and that, together with the nature of the results of radar sounding at the site and the proximity of surface crevassing due to the nearby boundary between ice shelf and coast, suggests that we drilled into a slush-filled basal crevasse. The radar sounding gave the strongest, but still weak, return from a depth of 314 m. This return we associate with the point at which hydraulic connection was made, that is, the top of the crevasse. On the basis of the CTD profiling, the overall ice thickness for the ice shelf at Fox 1 was estimated to be 383 m, with the base at a pressure of 329 dbar.

[12] The Fox-1 temperature profiles show that the water column becomes supercooled at a pressure of 385 dbar some 56 m below the ice shelf base. The degree of supercooling then increases as the ice base is approached, reaching a maximum of 0.035°C at the ice shelf base itself (at 329 dbar). The salinity profiles show several spikes in the upper part of the water column, which we ascribe to platelet ice passing through the conductivity sensors on the probe. If the amount of spiking indicates the concentration of platelet ice in the water column, then ice platelets in the water column in the vicinity of Fox 1 appear to be contained in a slurry within a meter or two of the ice shelf base.

[13] The pattern of melting, with probable freezing at the western end of the line of sites and a more intense zone of melting at the eastern end, is visible in the analysis by *Joughin and Padman* [2003]. They show a map of basal melting and freezing for the Filchner-Ronne Ice Shelf that was calculated using available fields of surface accumulation rate and ice thickness, together with satellite-derived ice velocity. Their calculation assumed the ice to be in steady state (that is, the ice thickness at point fixed with respect to the Earth to have a constant thickness), and was therefore fundamentally different than ours, but there is good qualitative agreement with our results.

[14] In a relatively cold regime (superheating less than ~0.5°C) the basal melt rate of an ice shelf can be related to the speed of water flow, $|\underline{u}|$, and the superheating, T_{sh}, by [*Nicholls et al.*, 2001]

$$w = \frac{|\underline{u}|\gamma_T T_{sh}}{aS_\infty \frac{\gamma_T}{\gamma_S} - \frac{L}{c_w} - \Delta T \frac{c_i}{c_w}}, \tag{1}$$

where γ_S and γ_T are the coefficients of salt and heat transfer, respectively, from water to ice [*Kader and Yaglom*, 1972]; $|\underline{u}|$ is the water speed below the boundary layer; S_∞ is the salinity below the boundary layer, the far-field salinity; a is the coefficient for the salinity term in the linearized formula for the freezing point of seawater; ΔT is $T_{\text{surface}} - T_{\text{base}}$, the difference between the temperatures at the upper and lower surfaces of the ice shelf; L is the latent heat of fusion of ice; and c_i and c_w are the specific heat capacities of ice and

Table 2. Values of Quantities in Equation (1) That Are Treated as Constants

Symbol	Value
γ_S	2.2×10^{-5}
γ_T	6.0×10^{-4}
L	3.35×10^5 J kg^{-1}
c_w	4000 J kg^{-1} °C^{-1}
c_i	2010 J kg^{-1} °C^{-1}
a	−0.0573°C

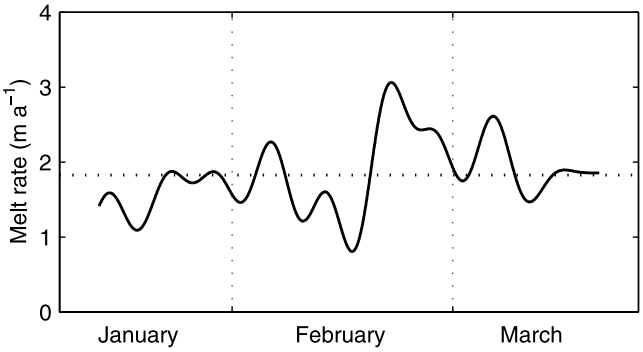

Figure 7. Low-pass filtered time series of basal melt rates at Fox 4, calculated using measured water temperature and water speed.

seawater. T_{sh} is the thermal driving, that is, the difference between the freezing point at the ice shelf base and the far-field in situ water temperature (the in situ temperature just beneath the boundary layer). The freezing point at the ice shelf base is calculated using the pressure at the base and the far-field salinity. Table 2 lists the values of quantities that we treat as constants in (1). The numerator in (1) represents the rate at which heat can be transferred across the boundary layer to the ice; the first term in the denominator represents the slowness of the transfer of salt across the boundary layer, and is a term that varies only weakly (note that a is negative); the second term represents the latent heat required to melt the ice and is the dominant term; the final term makes a minor contribution, and represents the heat required to warm the ice to its melting point.

[15] Equation (1) is based on the *Kader and Yaglom* [1972] parameterization for heat and salt transport across a neutral boundary layer. The value for $|\underline{u}|$ in the formula is for a point 1 m below the upper (ice) boundary. Fox 4 has temperature and conductivity sensors moored close to the base (7 m below), but the currents are measured in the middle of the water column. In order to use our current meter data to estimate the melt rate, w, the data need to be adjusted to account for the frictional slowing in the upper boundary layer. This is particularly important in this region, as the principal tidal constituents are semidiurnal and Fox 4 is near the M_2 critical latitude, resulting in a very thick boundary layer for the anticlockwise M_2 component [*Makinson*, 2002]. This means that had a current meter placed near the ice shelf base, it would have recorded a substantially reduced semidiurnal component. Modeling the development of the boundary layer using the methods described by *Makinson* [2002] shows that the tidal component of the water speed measured near the ice base would be 40% lower than that recorded by our instrument. Taking this into account, the melt rate was calculated and is shown in Figure 7. To make the calculation, the temperature and corrected speed data were used in their unsmoothed state; the smoothed melt rate is shown in Figure 7. The average estimated melt rate for the period of the time series is 1.8 ± 0.6 m yr^{-1}, where the standard deviation has been calculated using a version of the time series of meltrates that has been low-pass filtered using a 14-day cutoff, which is the period over which the direct (radar) measurement for this site was averaged. The meltrate calculated from the previous year's radar measurement is around 20% lower than we obtain from the oceanographic data, the discrepancy being easily explained by the variability in the oceanographic conditions during the measurement period at Fox 4, which is also consistent with the differences in the CTD profiles obtained at different times during the season from Fox 3.

4. General Hydrography and Circulation

[16] Figure 8 is a θ-S plot of the mean data obtained from the CTD profiling at each site, and helps show how the water masses observed at the four sites are related to each other. The data have been binned at 1-dbar intervals. Also shown in Figure 8 is the surface pressure freezing point (around −1.9°C) [*Millero*, 1978] and lines that indicate the trajectory taken in θ-S space by the properties of a parcel of water as it melts ice or as ice crystals form in the water column. These have been termed Gade lines, after *Gade* [1979].

4.1. Eastern End of Section

[17] From the mean velocity vectors shown in Figure 1, Fox 4 is in a region of inflow. From other data, we know that this inflow is associated with higher temperatures, lower salinity, and high melt rates. The ice shelf also shows a significant thinning in this region (Figure 1), presumably because of the inflow of relatively warm water. The θ-S diagram shows that the source water for the majority of the

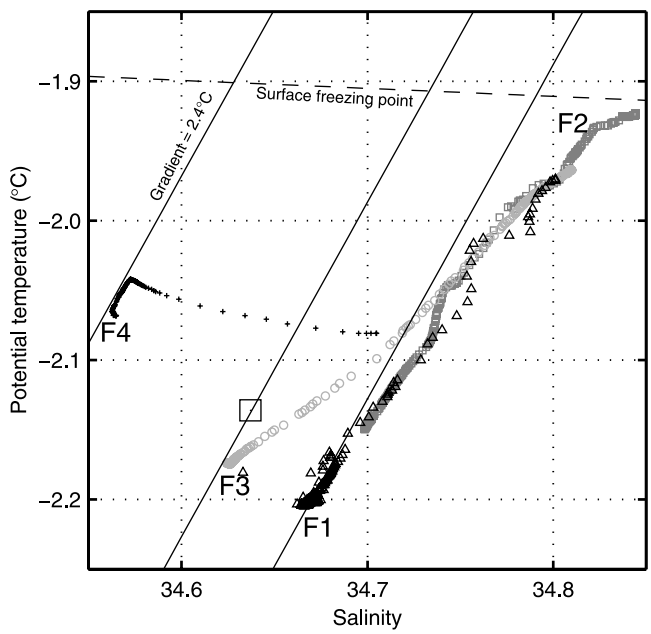

Figure 8. Plot of potential temperature against salinity. The data from each site were averaged and then binned in 1-m depth bins. From Fox 1 (F1) the data are represented by triangles, from Fox 2 (F2) by squares, from Fox 3 (F3) by circles, and from Fox 4 (F4) by crosses. The broken line is the surface pressure freezing point, and the solid lines are Gade lines (see main text). The single large square indicates the θ-S characteristics of the ISW plume observed at the ice front near FR5 (see Figure 1).

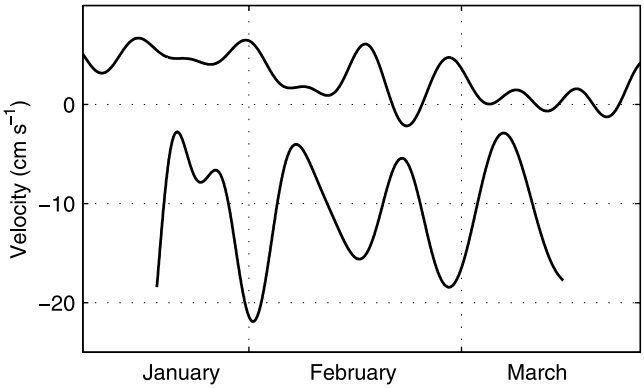

Figure 9. The component of current parallel to the axis of the Ronne Depression from the upper current meters at Fox 3 (upper curve) and Fox 4 (lower curve). These time series have been low-pass filtered to remove variability at timescales of less than 1 week.

Fox 4 water column has a relatively low salinity, and that the θ-*S* trajectory accurately follows the expected Gade characteristic, having a gradient of 2.4°C. If the source of the water observed at Fox 4 is HSSW from the ice front, then its salinity is given by the intersection between the Gade line and the surface freezing point line, that is, around 34.63. This is very much fresher than the source waters for Fox 1, 2, and 3, and must have its origins farther to the east along the ice front, where HSSW of lower salinity prevails [e.g., *Nicholls et al.*, 2003].

[18] Figure 9 (lower curve) shows the component of velocity resolved along the topography from the upper current meter at Fox 4. The time series has been low-pass filtered to remove diurnal and faster tidal components, revealing a strong 2-weekly modulation. This modulation is detected in tidal analysis of the 9-week-long record as a highly amplified M_{sf} component, with an amplitude of 8.5 and 4.6 cm s^{-1} in the upper and lower current meter records, respectively. The M_{sf} tide has the same frequency as the spring-neap variation due to the principal semidiurnal tides, M_2 and S_2, and so it is likely that the M_{sf}-frequency component measured at Fox 4 is being driven by the semidiurnal tide. *Makinson and Nicholls* [1999] show that the ridge delineating the eastern margin of the Ronne Depression is a region where their tidal model predicts a tidally rectified (Lagrangian) flow with a speed of about 2 cm s^{-1}. If the measured inflow velocity at Fox 4 (13.1 cm s^{-1}) were due entirely to tidal rectification, then the true Lagrangian velocity would be expected to be around one third lower, or about 9 cm s^{-1}. This is because the Stoke's Drift experienced by the water parcels [*Loder*, 1980] acts in the opposite direction to the Eulerian residual current measured by a current meter. As it is unlikely that the modeled residual would be wrong by a factor of 4, tidal rectification appears not to be able to explain the full strength of the inflow.

[19] The observations at Fox 4 might be explained by the presence of tidal fronts. *Robertson et al.* [1998], *Makinson and Nicholls* [1999], and *Joughin and Padman* [2003] point out that the region east of Ronne Depression is characterized by a thin water column, with tidal currents significantly higher than in the Ronne Depression itself. High basal melt rates resulting from the turbulent vertical transport of heat to the ice base produces a relatively fresh water column, which contrasts with the more saline conditions within the Ronne Depression. A tidal front between Fox 3 and Fox 4, whose strength was modulated by the spring-neap cycle, might explain both the strong 2-weekly modulation in the current and the broadly antiphase character of the variability at the two sites (Figure 9). The maxima in the observed velocity shear between Fox 3 and Fox 4 amounts to between 22 and 28 cm s^{-1} (Figure 9). For a geostrophically balanced flow it is easily shown that the difference in velocities parallel to, and on either side of, the front is given by $\sqrt{gH\Delta\rho/\rho}$, where g is the acceleration due to gravity, H is the water column thickness, $\Delta\rho$ is the density difference across the front, and ρ is the density of the ambient seawater [see, e.g., *Cushman-Roisin*, 1994, p. 242]. For a measured density difference of about 0.1 kg m^{-3}, and a water column thickness of about 100 m, this gives a velocity difference of around 30 cm s^{-1}. This might therefore explain the inflow at Fox 4, and the observed shear between Fox 3 and Fox 4.

[20] A 20-m-thick, high salinity layer was detected at the bottom at Fox 4 during the CTD profiling (Figure 3). The θ-*S* plot in Figure 8 shows this bottom layer to have characteristics closely related to those of the water column in the body of the Ronne Depression. A tidal front between Fox 3 and Fox 4 would be expected to migrate east and west as a result of cross-slope tidal advection. The salinity time series from the Microcat mounted 15 m above the seafloor at Fox 4 correlates strongly (correlation coefficient of 0.8) with the integrated cross-slope velocity measured at the site, showing that the foot of the tidal front periodically arrives at Fox 4. There is no such correlation at Fox 3, suggesting that the foot of the front generally remains within a few kilometers of Fox 4.

[21] The current meter data available for Fox 3 indicate that the well-defined layer of ISW in the upper part of the water column is flowing northward in the depression. A core of ISW has been observed at the ice front in the vicinity of FR5 (Figure 1) on every occasion that a ship has been able to obtain CTD measurements in the shorelead [e.g., *Gammelsrød et al.*, 1994]. These measurements have always been made during the late summer. On the basis of year-round mooring data from FR5 and FR6, *Nicholls et al.* [2003] suggested that the ISW core retreats beneath the ice shelf during winter. By plotting the θ-*S* characteristics of the ice front core on Figure 8 we can see that it is related, in a Gade sense, to the northward flowing ISW observed at Fox 3.

4.2. Western End of Section

[22] The most notable characteristic of the Fox 1 CTD data is the presence of strong freezing conditions at the top of the water column (Figure 3). One explanation might be that the freezing in some way results from the basal crevassing detected during the drilling operations, though it is not clear why the supercooling would extend so deeply (56 m) into the water column. It is more likely that there is a narrow ISW outflow along the coast, as yet undetected by ice front hydrographic surveys.

[23] It is instructive to calculate the minimum draft of ice shelf with which the water must have had contact in order to

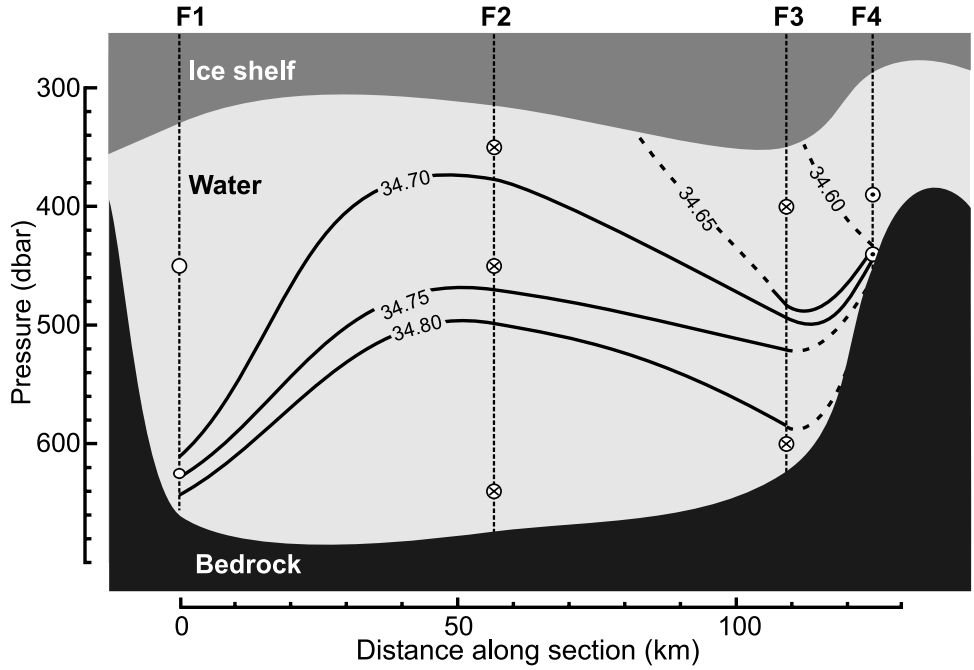

Figure 10. Salinity section along the Fox line using data from CTD profiles. Circles show the position of moored current meters; a cross in the circle indicates a positive V component (outflow along the depression), and a dot indicates inflow. Broken contours are speculative.

acquire the lowest temperature observed at Fox 1. The lowest in situ temperature measured at the site was −2.205°C. At an appropriate salinity of 34.68, this is the freezing point at a pressure of 400 dbar, or an ice shelf draft of 395 m. The formula $h = 0.108H + 17$ m relates the thickness, H, of Ronne Ice Shelf to its elevation, h [*Vaughan et al.*, 1995], and shows that a draft of 395 m corresponds to an ice shelf thickness of 462 m. The contours of ice shelf thickness shown in Figure 1 illustrate that the water at Fox 1 must have interacted with the ice base at least 70 km deeper into the cavity. A region of strong basal freezing is known to exist off Cape Zumberge (Figure 1), some 220 km along the coast, and it is possible that this is the source of the ISW layer at Fox 1 [*Corr et al.*, 1995; *Gerdes et al.*, 1999].

4.3. Circulation in the Body of the Ronne Depression

[24] Figure 10 shows contours of salinity derived from the CTD casts. The broken contours are speculative. As the salinity is the principal control on density in the very cold waters beneath ice shelves, Figure 10 may be regarded as a scaled version of the density section. Geostrophic considerations based on mean currents from current meters were used to help inform the drafting of the contours. Bearing in mind the effective barrier between Fox 3 and Fox 4 presented by the inferred tidal front, the salinity profiles from Fox 3 that were used in the construction of the salinity section were those obtained earlier in the season, as they were closest in time to the profiles from Fox 2 (see Figure 5).

[25] Outflowing (flow toward the ice front) ISW to the west of the pool of dense HSSW in the Ronne Depression (section 4.2), and inflowing low salinity HSSW to the east (section 4.1), each produce front-like structures. When coupled with the stratified water column between them, the fronts establish a circulation within the body of the depression, with velocities highest in the vicinity of the fronts, and distributed across the depression according to the disposition of the isopycnals. Using the density profiles from Fox 2, and Fox 3 (first visit), we calculate a baroclinic velocity profile that gives a velocity difference of 3 cm s^{-1} between the top and bottom of the water column, spatially averaged between the two sites. This is consistent with the 4 cm s^{-1} average difference between the upper and lower Fox 3 current meters for late December 2002, the month during which the CTD profiles were obtained.

[26] We now wish to trace the path of the flow in the interior of the Ronne Depression. The time series from the current meters at Fox 3 give a depth-averaged strength of 4.5 cm s^{-1} toward the ice front over the period of the time series (Table 1). The northern limb of the Ronne Depression circulation has been discussed by *Nicholls et al.* [2003]. They found a consistent flow along the ice front toward the Antarctic Peninsula, with the ISW core observed during the summer at the ice front on the eastern side of the depression re-entering the cavity at the western side. Ship-based hydrographic sections along the ice front, which have been obtained during the late summer, have never revealed a salinity section such as that shown in Figure 10. They generally show salinity increasing across the depression toward the Antarctic Peninsula, although *Nicholls et al.* [2003] present a salinity section obtained in the summer of 1997–1998, which shows a maximum in the salinity field around 20 km from the Antarctic Peninsula coast. Along the ice front it would appear that we see only the very northeastern periphery of the circulation in the Ronne Depression.

[27] As yet, we have no data from the Fox 1 mooring. As discussed above, the CTD data suggest that most of the

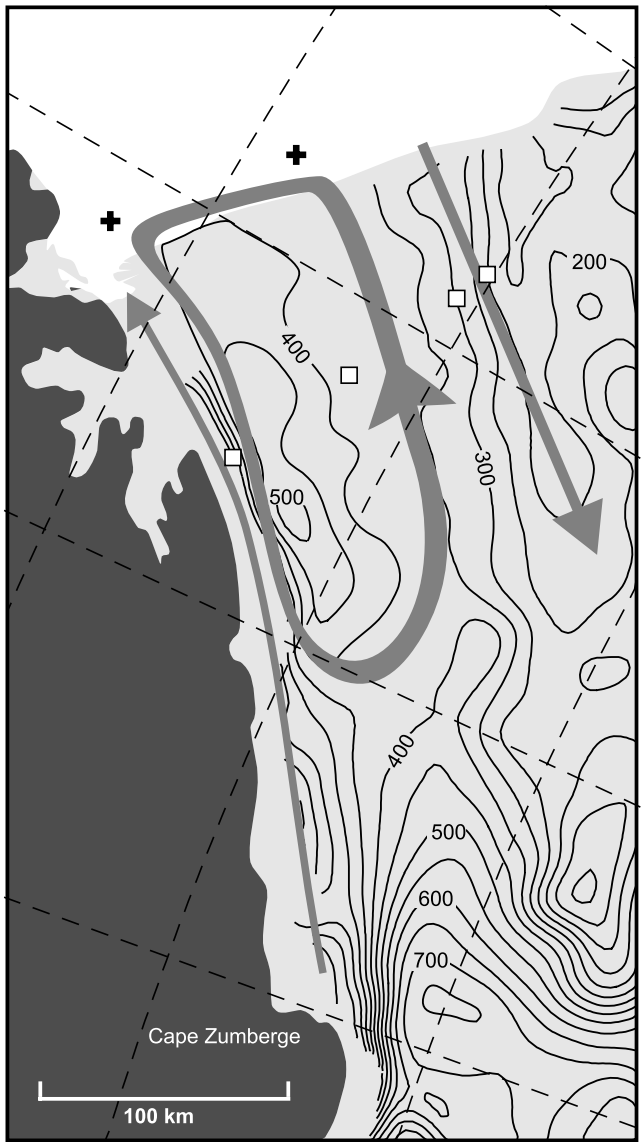

Figure 11. Map of the Ronne Depression, with contours indicating water column thickness [*Vaughan et al.*, 1994]. The contour interval is 50 m. Arrows show flows interpreted from the data.

water column at that site flows toward the ice front. However, data from the ice front mooring at FR6 (Figure 1) presented by *Nicholls et al.* [2003] show water flowing into the cavity at the western end of the ice front. Such an inflow is consistent with the dipping of the contours toward the west in Figure 10. A western, inward flowing limb of the Ronne Depression circulation must therefore lie between the outflowing waters at Fox 1 and the instruments at Fox 2. Below 610 dbar at Fox 1 a warmer, more saline layer was observed with the same θ-*S* characteristics as seen at Fox 2 (Figures 3 and 8). We suggest that this layer might represent the western margin of an inflow between the two sites.

[28] From the foregoing discussion, the stratification within the depression, the available data from the current meters, and the data obtained from just north of the ice front together suggest an anticyclonic circulation within the body of the Ronne Depression, bounded by an inflow of fresher water in the east, and an outflow of fresher water in the west. However, how is the circulation closed in the south? For flows with horizontal scales substantially larger than the internal Rossby radius of deformation (~3 km in the Ronne Depression), conservation of potential vorticity requires a purely barotropic current to be constrained to flow along *f*/*h* contours, where *f* is the Coriolis parameter, and *h* is the water column thickness. Over small variations in latitude, the *f*/*h* field is dominated by *h*, contours of which are plotted in Figure 11 [*Vaughan et al.*, 1994]. This map shows that between 75°20′S and 76°30′S in the Ronne Depression, there is a 150-km-long, elongated bowl in the water column thickness field, which would constrain a barotropic flow to take the form of a gyre. The anticyclonic circulation in the Ronne Depression includes a significant depth dependence in the velocity, and the degree to which it is constrained to follow contours of *h* is unclear. However, it is tempting to speculate that much of the flow follows the contours shown in Figure 11, to form a gyre in the northern portion of the depression. On the basis of the current meter data from Fox 3 and the density section through the Fox sites, we estimate a mean depth-average velocity between Fox 2 and Fox 3 of about 3 cm s^{-1}, giving a gyre strength of around 0.5 Sv. The data set is limited, and apart from the ice front moorings, we have no direct measurement of a net inflow between Fox 1 and Fox 2. However, the indirect evidence from θ-*S* properties, from the ice front and sub-ice shelf moorings, and from the regional topography, all point to an anticyclonic gyre during the middle to late summer.

[29] The contribution to the barotropic circulation that is made by winds blowing along the ice front is unclear. Most of the available evidence indicates that the prevailing winds at the western end of the ice shelf follow the line of the Antarctic Peninsula, blowing predominantly from the southwest as a barrier wind [e.g., *Schwerdtfeger*, 1984], and so we assume this to be a small component in the forcing of the local circulation.

4.4. HSSW Inflow

[30] Various authors have identified the Ronne Depression as being a likely inflow region for HSSW [*Foldvik and Gammelsrød*, 1988; *Jenkins et al.*, 2004]. Indeed, *Nicholls* [1996] shows CTD data from deeper in the Ronne Depression indicating the presence of unmodified HSSW at the bottom of the water column. It is therefore interesting to note that none of the measurements made along the Fox section, just 40 km from the ice front at the closest point, revealed water with temperatures as high as the surface freezing point (Figure 8). That is, no HSSW was detected at any of the sites. It is possible that there is an HSSW inflow trapped against the eastern slope of the Ronne Depression, between Fox 3 and Fox 4, as hinted at by the upsloping isohalines (and therefore isopycnals) between the two sites in Figure 10. An alternative is that HSSW flows on the inward limb of the proposed gyre, between Fox 1 and Fox 2. Indeed, the warmest water measured was observed in the lower layer at Fox 2. Answers to the questions of when and how HSSW inflow occurs will have to wait until the technical problems with the instrument moorings are resolved.

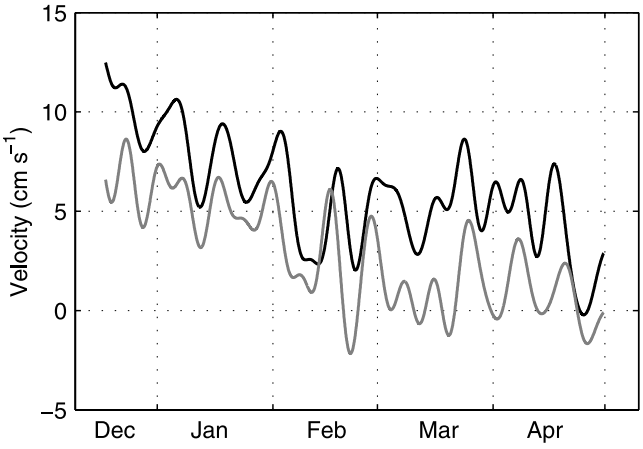

Figure 12. Filtered *v* (along depression) components from the upper (shaded) and lower (black) current meters at Fox 3, showing long-term variability.

[31] The CTD measurements presented here were made during the late summer, and the time series available from the moored instruments, ended shortly after the beginning of winter. Strong seasonality is expected in the Ronne Depression [e.g., *Nicholls*, 1996], and it is quite likely that there will be significant changes in the oceanographic pattern along the Fox section during the year. An indication of long-term variability is visible in the currents measured at Fox 3. Figure 12 shows the along-depression current components obtained at the site. The data have been filtered to remove variability at timescales shorter than around a week. The figure shows a reduction in mean flow velocity by a factor of 2 between the start of the time series and early February. From there until the end of the time series the mean velocity remains very low in the upper part of the water column. Deeper in the water column, the velocity remains stable at around 5 cm s^{-1} before appearing to drop again toward the end of the record. We assume the reduction in mean flow speeds to be associated with the change in conditions noted above between the two sets of CTD profiles obtained from that site during the season.

5. Summary

[32] Four oceanographic sites over the northern Ronne Depression were established between mid-November 2002 and early February 2003. The sites were established by drilling access holes through Ronne Ice Shelf about 50 km inshore of the ice front. We have presented CTD profiles from all of the sites, and time series between 9 and 20 weeks in length from instruments moored at three of the sites. On the basis of these and previously reported data, we have inferred the probable pattern of water flows that existed in the northern Ronne Depression during the period of the measurements, and this pattern has been sketched in Figure 11. The principal findings were as follows.

[33] There is a strong inflow of relatively fresh water directly from the ice front and along the submarine ridge that delineates the eastern boundary of Ronne Depression. This water has a salinity suggesting that it originates from over the continental shelf east of Ronne Depression, and it is separated from the waters of the Ronne Depression by a tidal front. At the measurement site (Fox 4) the inflowing water has a temperature around 0.053°C higher than the freezing point at the ice shelf base, and is able to power a basal melt rate of 1.8 ± 0.6 m yr^{-1}. Radar measurements at the same site yielded a melt rate averaged over the second half of January 2002 of 1.41 ± 0.08 m yr^{-1}, consistent with the variability deduced from the oceanographic measurements. The region of the inflow is characterized by a zone of relatively thin ice, which we assume to be a result of the rapid basal melting. There is an outflow of ISW at the western boundary of the depression, along the Antarctic Peninsula coast, which might originate from the strong freezing zone off Cape Zumberge some 220 km along the coast.

[34] The circulation that occupies the Ronne Depression between the western outflow and the eastern inflow has a baroclinic component superimposed on an anticyclonic depth-independent flow that is bounded in the north by the ice front. We speculate that the depth-independent flow takes the form of a gyre, associated with a known basin in the topography of water column thickness. The circulation in the body of the depression is driven by east-west density gradients established by the relatively fresh conditions at the eastern and western margins that result from the ISW outflow in the west and the relatively warm and fresh inflow in the east. It is possible that a contribution to a barotropic component of the circulation is made by winds blowing along the ice front, although this is not thought to play a large role.

[35] By establishing the relatively complex summertime circulation in the vicinity of one of the primary inflow regions for HSSW, we have begun the process of determining the controls on the ventilation of the sub-ice shelf cavity. This will ultimately help in the prediction of how the ice shelf–ocean system, and its contribution to the formation of deep and bottom waters, will respond to changes in climate.

[36] **Acknowledgments.** The authors would like to thank Laurie Padman and three anonymous reviewers for their many helpful comments on the manuscript.

References

Corr, H., M. Popple, and A. Robinson (1995), Airborne radio echo investigations of a marine ice body, in *Filchner Ronne Ice Shelf Programme Report*, vol. 9, edited by H. Oerter, pp. 14–17, Alfred-Wegener-Inst. for Polar and Mar. Res., Bremerhaven, Germany.

Corr, H., A. Jenkins, K. Nicholls, and C. S. M. Doake (2002), Precise measurement of changes in ice-shelf thickness by phase-sensitive radar to determine basal melt rates, *Geophys. Res. Lett.*, *29*(8), 1232, doi:10.1029/2001GL014618.

Cushman-Roisin, B. (1994), *Introduction to Geophysical Fluid Dynamics*, 320 pp., Prentice-Hall, Old Tappan, N. J.

Foldvik, A., and T. Gammelsrød (1988), Notes on southern-ocean hydrography, sea-ice and bottom water formation, *Palaeogeogr. Palaeoclimatol. Palaeoecol.*, *67*, 3–17.

Foldvik, A., T. Gammelsrød, and T. Tørresen (1985), Circulation and water masses on the Southern Weddell Sea Shelf, in *Oceanology of the Antarctic Continental Shelf*, *Antarct. Res. Ser.*, vol. 43, edited by S. S. Jacobs, pp. 5–20, AGU, Washington, D. C.

Gade, H. G. (1979), Melting of ice in sea water: A primitive model with application to the Antarctic ice shelf and icebergs, *J. Phys. Oceanogr.*, *9*, 189–198.

Gammelsrød, T., A. Foldvik, O. A. Nøst, Ø. Skagseth, L. G. Anderson, E. Fogelqvist, K. Olsson, T. Tanhua, E. P. Jones, and S. Østerhus (1994), Distribution of water masses on the continental shelf in the southern

Weddell Sea, in *The Polar Oceans and Their Role in Shaping the Global Environment*, *Geophys. Monogr. Ser.*, vol. 85, edited by O. M. Johannessen, R. D. Muench, and J. E. Overland, pp. 159–176, AGU, Washington, D. C.

Gerdes, R., J. Determann, and K. Grosfeld (1999), Ocean circulation beneath Filchner-Ronne Ice Shelf from three-dimensional model results, *J. Geophys. Res.*, *104*, 15,827–15,842.

Jenkins, A., D. M. Holland, K. W. Nicholls, M. Schröder, and S. Østerhus (2004), Seasonal ventilation of the cavity beneath Filchner-Ronne Ice Shelf simulated with an isopycnic coordinate ocean model, *J. Geophys. Res.*, *109*, C01024, doi:10.1029/2001JC001086.

Joughin, I., and L. Padman (2003), Melting and freezing beneath Filchner-Ronne Ice Shelf, Antarctica, *Geophys. Res. Lett.*, *30*(9), 1477, doi:10.1029/2003GL016941.

Kader, B. A., and A. M. Yaglom (1972), Heat and mass transfer laws for fully turbulent wall flows, *Int. J. Heat Mass Transfer*, *15*, 2329–2351.

Loder, J. W. (1980), Topographic rectification of tidal currents on the sides of Georges Bank, *J. Phys. Oceanogr.*, *10*, 1399–1416.

Lythe, M. B., and D. G. Vaughan (2001), BEDMAP: A new ice thickness and subglacial topographic model of Antarctica, *J. Geophys. Res.*, *106*, 11,335–11,351.

Makinson, K. (2002), Modeling tidal current profiles and vertical mixing beneath Filchner-Ronne Ice Shelf, Antarctica, *J. Phys. Oceanogr.*, *32*, 202–215.

Makinson, K., and K. W. Nicholls (1999), Modeling tidal currents beneath Filchner-Ronne Ice Shelf and on the adjacent continental shelf: their effect on mixing and transport, *J. Geophys. Res.*, *104*, 13,449–13,465.

Millero, F. J. (1978), Freezing point of sea water: Eighth report of the Joint Panel of Oceanographic Tables and Standards, Appendix 6, *UNESCO Tech. Pap. Mar. Sci.*, *28*, 29–31.

Nicholls, K. W. (1996), Temperature variability beneath Ronne Ice Shelf, Antarctica, from thermistor cables, *J. Geophys. Res.*, *101*, 1199–1210.

Nicholls, K. W., S. Østerhus, K. Makinson, and M. R. Johnson (2001), Oceanographic conditions south of Berkner Island, beneath Filchner-Ronne Ice Shelf, Antarctica, *J. Geophys. Res.*, *106*, 11,481–11,492.

Nicholls, K. W., L. Padman, M. Schröder, R. A. Woodgate, A. Jenkins, and S. Østerhus (2003), Water mass modification over the continental shelf north of Ronne Ice Shelf, Antarctica, *J. Geophys. Res.*, *108*(C8), 3260, doi:10.1029/2002JC001713.

Robertson, R., L. Padman, and G. D. Egbert (1998), Tides in the Weddell Sea, in *Ocean, Ice, and Atmosphere: Interactions at the Antarctic Continental Margin*, *Antarct. Res. Ser.*, vol. 75, edited by S. S. Jacobs and R. Weiss, pp. 341–369, AGU, Washington, D. C.

Schwerdtfeger, W. (1984), *Weather and Climate of the Antarctic*, 261 pp., Elsevier Sci., New York.

Thyssen, F., A. Bombosch, and H. Sandhäger (1993), Elevation, ice thickness and structure mark maps of the central part of the Filchner-Ronne ice shelf, *Polarforschung*, *62*, 17–26.

Vaughan, D. G., J. Sievers, C. S. M. Doake, G. Grikurov, H. Hinze, V. S. Pozdeev, H. Sandhäger, H. W. Schenke, A. Solheim, and F. Thyssen (1994), Map of subglacial and seabed topography 1:2000000 Filchner-Ronne-Schelfeis, Antarktis, map, Inst. für Angew. Geod., Frankfurt, Germany.

Vaughan, D. G., J. Sievers, C. S. M. Doake, H. Hinze, D. R. Mantripp, V. S. Pozdeev, H. Sandhäger, H. W. Schenke, A. Solheim, and F. Thyssen (1995), Subglacial and seabed topography, ice thickness and water column thickness in the vicinity of Filchner-Ronne-Schelfeis, Antarctica, *Polarforschung*, *64*, 75–88.

K. Makinson and K. W. Nicholls, British Antarctic Survey, Natural Environmental Research Council, Madingley Road, Cambridge CB3 0ET, UK. (kwni@bas.ac.uk)

S. Østerhus, Bjerknes Centre for Climate Research, University of Bergen, Bergen, Norway.